Amplitude and phase locking of mechanical oscillation driven by radiation pressure

Yi Wu,[1] Gang Li,[1] Bing He,[2,*] and Qing Lin[1,†]

[1]*Fujian Key Laboratory of Light Propagation and Transformation, College of Information Science and Engineering, Huaqiao University, Xiamen 361021, China*

[2]*Center for Quantum Optics and Quantum Information, Universidad Mayor, Camino La Pirámide 5750, Huechuraba, Chile*

(Received 10 October 2021; revised 24 November 2021; accepted 10 January 2022; published 20 January 2022)

Cavity optomechanical systems have been widely studied for many of their interesting properties, which can be interpreted with their linearized dynamics. Previously, the genuine nonlinear dynamics of optomechanical systems was only considered for very few phenomena such as self-induced oscillation and optomechanical chaos. Beyond the scope of those previous studies, a phenomenon of frozen mechanical oscillation irrespective of the intensity variation on the driving fields was recently discovered for an optomechanical system under two pump fields having their frequencies properly matched [He *et al.*, Phys. Rev. A **102**, 011503(R) (2020)]. Here we significantly advance the study by showing that similar phenomena can manifest under more general conditions for the external driving fields. The mechanical oscillation in such doubly driven optomechanical systems can be locked in either its amplitude or both amplitude and phase. Simultaneous amplitude and phase locking is possible under a specific condition for the difference of the drive frequencies, whenever the drive intensity is sufficiently high. The variations of the phenomena also exist in two coupled cavities containing one mechanical breathing mode.

DOI: 10.1103/PhysRevA.105.013521

I. INTRODUCTION

In recent years optomechanical systems (OMSs) have attracted a huge amount of attention for their interesting properties. The radiation pressure created by a laser pump plays a crucial role in OMSs, being the origin of the nonlinearity for such systems [1]. The dynamics induced by a red-detuned pump field can realize optomechanical cooling to macroscopic quantum states [2–31]. On the other hand, optomechanical entanglement can be generated under certain conditions [32–48] and could be applied to test the boundary between classical and quantum realms [49–51]. These two primary topics in the current research of OMSs can be understood by the linearization of the system dynamics around an equilibrium point [1] or by other methods [52]. However, if a blue-detuned driving field becomes sufficiently strong, some phenomena that must be interpreted with genuine optomechanical nonlinearity will appear. For example, the dynamical multistability of self-induced oscillation has been explored with a stronger laser pump [53–57]. A sudden transition between two mechanical oscillations can also take place due to the optomechanical nonlinearity in a coupled-cavity system [58]. The present work considers another type of nonlinear optomechanical phenomenon: the locking of the mechanical oscillation under two simultaneously acting drives with their matched frequencies. Such a phenomenon was recently shown to exist in a doubly driven OMS, given one pumping field red detuned by the mechanical frequency, together with another one with the resonant frequency of the optical cavity [59].

When the above-mentioned phenomenon of frozen mechanical oscillation takes place, the amplitude, frequency, and phase of the mechanical resonator in an OMS will simultaneously remain unchanged even if one adjusts the pump power of the external fields over a considerable range. The frozen mechanical motion will be maintained until there is a sudden random jump to another frozen state due to the further enhanced drive power. The mechanical motion of the OMS thus appears to be located on a series of fixed orbits like energy levels [59]. If the cavity field and mechanical resonator of the OMS are modeled by two harmonic oscillators, respectively, such a phenomenon can be viewed as a synchronization process for these two oscillators, during which the motion of one oscillator (the mechanical resonator) is completely locked. Synchronization is a traditional research topic in nonlinear dynamics [60–63], which dates back to the 17th century [64]. Nowadays, the study of synchronization has been well developed to chaotic systems [65,66], complex networks [67–69], and many other biological, chemical, and physical systems with their fascinating features, promising applications in many different areas [70–78].

Synchronization of two oscillating objects generally refers to the same pace of their phases and/or oscillation periods. If their coupling strength is relatively strong, two oscillating objects can be synchronized for their amplitude contours [61,79,80]. Compared to other synchronization phenomena, the novelty of the scenario in Ref. [59] is that the three elements of an oscillation, i.e., the amplitude, frequency, and phase, can be simultaneously locked for one of the coupled oscillators in the synchronization process. In Ref. [59], the

*bing.he@umayor.cl
†qlin@hqu.edu.cn

locking phenomenon was found to take place when one of the driving fields is red detuned exactly by the mechanical frequency, while the other field is a fixed to be resonant with the intrinsic cavity frequency. However, this combination of drive frequencies is not unique for realizing the mechanical locking, and the scenario in Ref. [59] is only a special case of the phenomenon. One purpose of the present work is to clarify the general frequency-matched condition for the driving fields to lock the mechanical oscillation under radiation pressure. We will also illustrate how a partial locking of the mechanical motion (only locking the oscillation amplitude) can exist under many other conditions.

The rest of the paper is organized as follows. In Sec. II the system dynamics of the systems we consider is illustrated with detailed models. Based on the exact simulation with the dynamical equations, a partially locked mechanical oscillation only in the amplitude is discussed in Sec. III, where the action of only one resonant drive is considered. The main results of the locking phenomenon due to various combinations of the driving frequencies are presented in Sec. IV, which also highlights a special pattern of frozen mechanical oscillation. In Sec. V we continue to discuss similar phenomena occurring in a coupled-cavity system. We conclude in Sec. VI with a discussion and summary. The article also includes an Appendix, which explains the phenomena considered in an alternative way.

II. SYSTEM DYNAMICS LEADING TO LOCKED OSCILLATIONS

Though the OMS can have many different forms [1], we use a Fabry-Pérot-type one with a movable mirror to represent the systems considered, as in Fig. 1(a). The two external driving fields can be simplified by one field with two tones, which has the frequency components ω_{L_1} and ω_{L_2} [or their detuning points Δ_1 and Δ_2 away from the cavity resonance frequency] and the amplitude components E_1 and E_2. The radiation pressure created by the pump field produces an interaction potential

$$V_{\rm int} = -g_m X_m \left(X_c^2 + P_c^2\right)/2 \tag{1}$$

between two harmonic oscillators that model the cavity field and mechanical resonator, respectively. It couples the cavity field, with X_c and P_c its perpendicular quadratures and ω_c its intrinsic frequency, to the mechanical resonator with its frequency ω_m, displacement X_m, and momentum P_m. This potential is proportional to a small optomechanical constant g_m. In terms of the dimensionless variables (X_c, P_c and X_m, P_m), the dynamical equations of the system read

$$\begin{aligned}
\dot{X}_c &= -\kappa X_c - g_m X_m P_c + \sum_{i=1,2} \sqrt{2} E_i \cos(\Delta_i t), \\
\dot{P}_c &= -\kappa P_c + g_m X_m X_c + \sum_{i=1,2} \sqrt{2} E_i \sin(\Delta_i t), \\
\dot{X}_m &= \omega_m P_m, \\
\dot{P}_m &= -\omega_m X_m - \gamma_m P_m + g_m \left(X_c^2 + P_c^2\right)/2.
\end{aligned} \tag{2}$$

The term $\mathcal{E}_c = (X_c^2 + P_c^2)/2$ in the last equation is the cavity photon number, which is proportional to the force acting on the mechanical resonator. Here the equations about the cavity part are given in the observational frame rotating at the cavity frequency ω_c, so only the detuning $\Delta_{1\,(2)} = \omega_c - \omega_{L_{1\,(2)}}$ of a drive component appears. The mechanical damping rate γ_m in many types of OMSs can be much smaller than the cavity damping rate κ [1], which is used to scale the other system parameters in our numerical simulations. Because the realistic mechanical frequency ω_m is also much smaller than the cavity resonance frequency ω_c, the powers $\hbar\omega_{L_i}E^2/\kappa$ $(i = 1, 2)$ of the two drive components or two driving fields are almost the same under the condition $E_1 = E_2 = E$, even if their respective detuning points can differ by a few times ω_m.

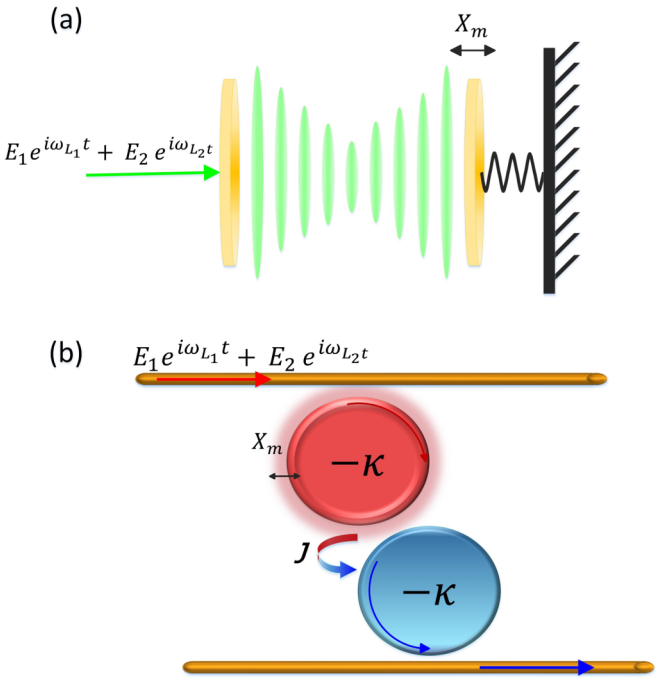

FIG. 1. Representative setups illustrating the mechanical locking phenomena in OMSs. (a) Simple OMS in the form of a Fabry-Pérot cavity with a movable mirror as the mechanical oscillator. (b) Coupled-cavity system of microtoroids. One of them has its breathing mechanical modes excited to a sustainable oscillation. The other couples to the former with coupling strength J. The mechanical oscillation $X_m(t)$ in the systems can be locked irrespective of the drive amplitudes.

Another type of system we consider is constructed with two coupled whispering-gallery-mode microresonators, among which one has a breathing mechanical mode excitable by the driving field. Considering the adjustable coupling strength J between the two microresonators, one can describe the dynamics with the interaction potential

$$V_{\rm int} = -g_m X_m \left(X_{c_1}^2 + P_{c_1}^2\right)/2 + J\left(X_{c_1} X_{c_2} + P_{c_1} P_{c_2}\right). \tag{3}$$

The corresponding dynamical equations for the system with two more degrees of freedom become

$$\begin{aligned}
\dot{X}_{c_1} &= -\kappa X_{c_1} - g_m X_m P_{c_1} + J P_{c_2} + \sum_{i=1,2} \sqrt{2} E_i \cos(\Delta_i t), \\
\dot{P}_{c_1} &= -\kappa P_{c_1} + g_m X_m X_{c_1} - J X_{c_2} + \sum_{i=1,2} \sqrt{2} E_i \sin(\Delta_i t),
\end{aligned}$$

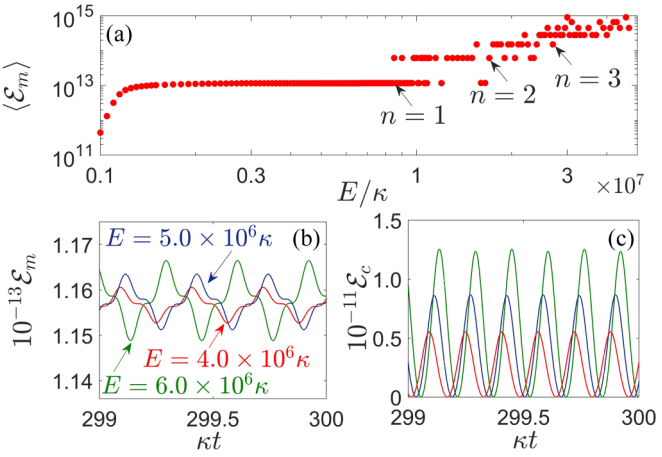

FIG. 2. Amplitude locking under a single resonant drive. (a) Distribution of the time-average mechanical energy $\langle\mathcal{E}_m\rangle$ with increasing drive amplitude E. A logarithmic coordinate is used to show the energy-level positions. Also shown are detailed views of the stabilized patterns of (b) the mechanical energy and (c) the cavity energy on the level $n=1$. The system parameters are scaled with respect to the cavity damping rate κ as $g_m/\kappa=10^{-5}$ and $\omega_m/\kappa=20$, and the mechanical quality factor is $Q=\omega_m/\gamma_m=10^6$.

$$\begin{aligned}
\dot{X}_m &= \omega_m P_m,\\
\dot{P}_m &= -\omega_m X_m-\gamma_m P_m+g_m\left(X_{c_1}^2+P_{c_1}^2\right)/2,\\
\dot{X}_{c_2} &= -\kappa X_{c_2}+JP_{c_1},\\
\dot{P}_{c_2} &= -\kappa P_{c_2}-JX_{c_1}.
\end{aligned}\tag{4}$$

We will also study the locking phenomena in this type of system. In what follows, we will apply the numerical simulations to illustrate how the locking phenomena considered arise in the systems described by Eqs. (2) and (4).

III. AMPLITUDE LOCKING UNDER ONE RESONANT DRIVING FIELD

The previously discovered locking scenario is realized by the cooperation of two driving fields, one resonant and one red detuned by the mechanical frequency ω_m [59]. There actually exist more manifestations of such a phenomenon if given many other choices of the driving fields. To have a systematic view of these locking processes, we start from the situation of only one resonant driving field with $\Delta=0$, which is the basis for all locking phenomena we are going to discuss. When this driving field is sufficiently strong, the stabilized mechanical motion will be located on discrete states like energy levels [59]. With a set of exemplary system parameters, the levels are distributed with the dimensionless drive amplitude E/κ as in Fig. 2(a). Beyond a threshold at $E/\kappa\approx1.5\times10^6$, which is found with the system parameters used for the figure, the average mechanical energy will be frozen on the level $n=1$, independently of increasing the drive power (the average mechanical energy remains unchanged even close to $E/\kappa=10^7$).

Together with the discussion of the locking phenomenon, we provide some facts about and notation for the stabilized mechanical motion in the OMS we consider. In all situations we consider in the present work, the OMS is totally dynamical with an oscillating cavity field and mechanical resonator (mechanical oscillator). There are sidebands with their peaks centered at $n\omega_m$ (n is an integer) in a stabilized cavity photon number $\mathcal{E}_c=(X_c^2+P_c^2)/2$ proportional to the cavity field energy by a factor $\hbar\omega_c$. Among them, only the first sideband peaked at the mechanical frequency ω_m significantly influences the mechanical motion since it provides the only driving force that is resonant with the mechanical frequency. As a result, the stabilized mechanical motion in all our situations considered takes a rather simple form

$$X_m(t)=A\cos(\omega_m t+\phi)+d,\tag{5}$$

where the pure displacement away from the equilibrium position without radiation pressure is much smaller than the oscillation amplitude, i.e., $d\ll A$. The corresponding phonon number, which is proportional to the mechanical energy (up to a factor $\hbar\omega_m$), is therefore

$$\begin{aligned}
\mathcal{E}_m(t) &= \left[X_m^2(t)+P_m^2(t)\right]/2\\
&= A^2/2+d^2/2+Ad\cos(\omega_m t+\phi)\\
&\quad +A(\dot{d}/\omega_m)\sin(\omega_m t+\phi)+\dot{d}^2/2\omega_m^2.
\end{aligned}\tag{6}$$

The positions of the energy levels in Fig. 2(a) are those of the average mechanical energy

$$\langle\mathcal{E}_m(t)\rangle=A_n^2/2+\langle d^2\rangle/2\approx A_n^2/2.\tag{7}$$

These energy levels correspond to the discrete amplitudes A_n ($n\geqslant1$ as the integers) of the mechanical resonator. In other words, the amplitude of the stabilized mechanical oscillation is locked to one of these fixed values and the change of the oscillation amplitude takes the form of a transition between the energy levels. In terms of the mechanical displacement $X_m(t)$, the amplitude locking is simply exhibited as a fixed amplitude for the stabilized mechanical oscillation, as shown in Fig. 9(a) of the Appendix.

On each of the discrete levels, the oscillation phase ϕ in Eq. (5) is not fixed at all. One example is in Fig. 2(b), where it can be seen that ϕ definitely changes with the drive amplitude E. In the current situation of a resonant driving field, the pure displacement d of the mechanical resonator is relatively large and becomes time dependent, as a result of a stronger driving force $g_m(X_c^2+P_c^2)/2$ from the resonant pump. Then the numerically simulated contours for the oscillatory mechanical energy with the amplitudes $A_n\sqrt{d^2+(\dot{d}/\omega_m)^2}\approx A_n d$ display the higher harmonic components as in Fig. 2(b). The displacement d also slightly increases with the drive amplitude E, giving a larger amplitude $A_n d$ for the mechanical energy in Eq. (6). However, due to the amplitude-locking mechanism, the time-averaged mechanical energy $\langle\mathcal{E}_m(t)\rangle=A_n^2/2$ is almost fixed on each level $n\geqslant1$. The more energy added into the system due to an enhanced drive amplitude E predominantly stays in the cavity field, having the cavity photon number $\mathcal{E}_c=(X_c^2+P_c^2)/2$ to grow proportionally as in Fig. 2(c).

The higher mechanical energy levels $n\geqslant2$ manifest when the drive amplitude is enhanced further on the right side of Fig. 2(a). In this regime it seems that all these discrete levels overlap with one another. Viewed on a refined scale, however,

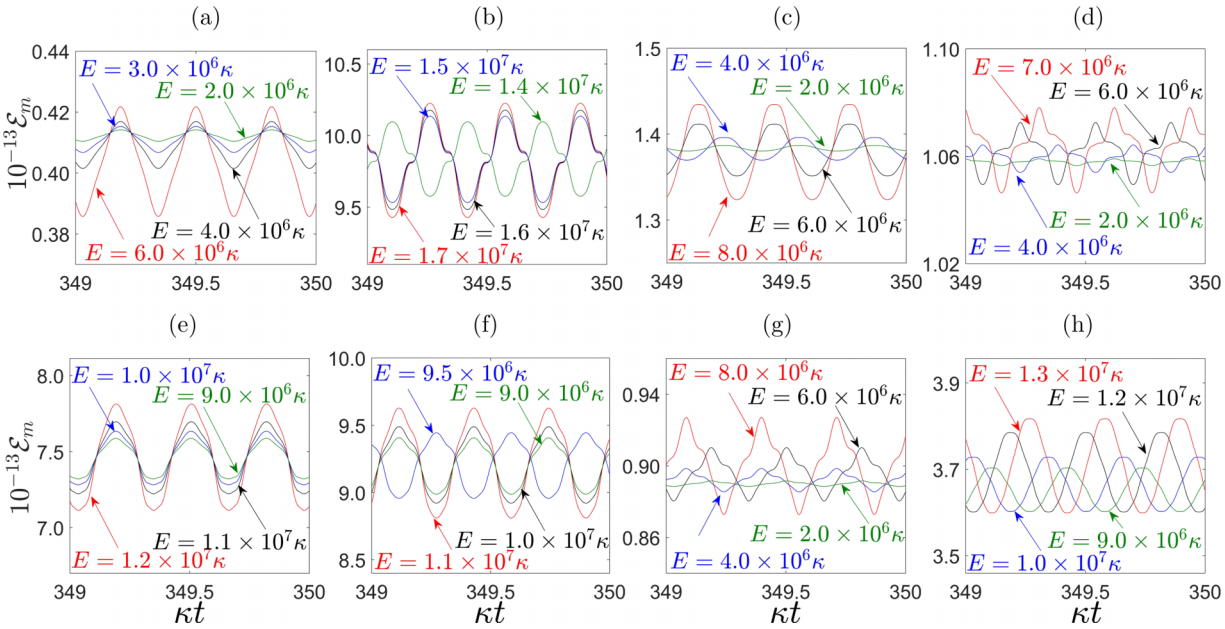

FIG. 3. Oscillation patterns for the stabilized mechanical energy under various combinations of two driving field frequencies: (a) $\Delta_1 = 0$ and $\Delta_2 = \omega_m$, (b) $\Delta_1 = -\omega_m$ and $\Delta_2 = \omega_m$, (c) $\Delta_1 = -\omega_m$ and $\Delta_2 = 2\omega_m$, (d) $\Delta_1 = 0$ and $\Delta_2 = 4\omega_m$, (e) $\Delta_1 = 0.5\omega_m$ and $\Delta_2 = 1.5\omega_m$, (f) $\Delta_1 = 0.6\omega_m$ and $\Delta_2 = 2.6\omega_m$, (g) $\Delta_1 = 0.1\omega_m$ and $\Delta_2 = 3.1\omega_m$, and (h) $\Delta_1 = 0.2\omega_m$ and $\Delta_2 = 4.2\omega_m$. Here all stabilized oscillations are on the first energy level. (a)–(d) The detuning points of the two driving fields are exactly on the integer times of the mechanical frequency ω_m. (e)–(h) The frequencies of the driving fields are displaced in parallel to keep their difference only. Both amplitude and phase locking only manifest in (a) and (e). The system parameters are the same as those in Fig. 2.

there is still a one-to-one correspondence between the mechanical energy $\langle\mathcal{E}_m\rangle$ and drive amplitude E (for more details see Ref. [59]). A slight variation of the drive amplitude E, as well as the choice of the initial condition and the perturbation from the noises, can make the system evolve randomly to a different level in the regime. These energy levels differ from the previously studied dynamical multistability of self-sustained oscillation [53–57] by two facts. A self-sustained oscillation occurs when a blue-detuned pump field becomes stronger over a threshold. As a supercritical Hopf bifurcation, the evolved limit cycle of the mechanical oscillator (or the stabilized mechanical amplitude) grows continuously with the drive amplitude E. In contrast, the frozen amplitude A_n in the scenarios we consider does not change with E on each energy level. The second difference is just the high sensitivity to the external parameters in the evolution to the higher levels $n \geqslant 2$; unlike the commonly known bifurcations, the transition between the evolved energy levels can become highly random.

There is one missing piece to compare the current dynamical scenario with the one in Ref. [59], where another cooling field detuned at $\Delta = \omega_m$ simultaneously acts on the OMS. As the cooling field gradually becomes as strong as the resonant one, the mechanical oscillation phase in Eq. (5) will also be frozen to a fixed value ϕ_n on each level $n \geqslant 1$. We call it a complete locking of the mechanical oscillation, which has the simultaneously frozen amplitude and phase. The cooling field will also lower the threshold value of the pump power for the system to enter the regime of locked oscillation. Given the system parameters in Fig. 2, for example, the threshold will be lowered from $E \approx 1.5\times10^6\kappa$ in Fig. 2(a) to $E \approx 5\times10^5\kappa$ under the joint action of the two fields. The complete locking to both fixed A_n and ϕ_n is a more interesting scenario that occurs in the doubly driven OMS. We will explore the general condition for its realization in the next section.

IV. COMBINATION OF COMPLETE AND PARTIAL LOCKING PHENOMENA

A. Drive frequencies difference by integer multiples of ω_m

Based on a resonant drive, the simultaneous freezing of A and ϕ will be realized by adding another red-detuned driving field with $\Delta_2 = \omega_m$. One example is in Fig. 3(a), where the average positions of stable mechanical energy are on the same level except for a slight deviation when the drive amplitude E is high ($E = 6.0\times10^6\kappa$ in the figure) to cause a slight deformation of the energy level. In this situation all stabilized mechanical oscillations have the same phase ϕ_n on each energy level, so the correspondingly stabilized phonon numbers $\mathcal{E}_m(t)$ also oscillate at the same phase. In the illustration of the phase locking, the reason for us to use the stabilized phonon number proportional to the mechanical energy rather than the stabilized $X_m(t)$ is that the evolved $\mathcal{E}_m(t)$ with its oscillation amplitude $A_n d$ is much easier to distinguish for the different drive amplitudes E, which cause the varied pure displacement d. In the Appendix we also display such a phase-locking phenomenon in Figs. 9(c) and 9(d), where the stabilized $X_m(t)$ for different drive amplitudes E almost overlap with one another because their varied pure displacements d are negligible compared to the frozen amplitude A_1. Moreover, if one applies another blue-detuned field with $\Delta_2 = -\omega_m$, instead of the red-detuned one $\Delta_2 = \omega_m$ in Ref. [59], the simultaneous amplitude and phase locking will nonetheless

TABLE I. Drive-frequency-matched conditions for realizing the complete and partial locking phenomena. Note that the phenomena still exist under the parallel displacements $\Delta_1 \to \Delta_1 + \delta$ together with $\Delta_2 \to \Delta_2 + \delta$.

Drive condition	Amplitude locking	Phase locking
$\lvert\Delta_1 - \Delta_2\rvert = \omega_m$	yes	yes
$\lvert\Delta_1 - \Delta_2\rvert = 2\omega_m$	yes	no
$\lvert\Delta_1 - \Delta_2\rvert = 3\omega_m$	yes	no
$\lvert\Delta_1 - \Delta_2\rvert = 4\omega_m$	yes	no

manifest when the driving fields are sufficiently strong. Once the drive amplitude $E_1 = E_2 = E$ goes beyond the thresholds for these situations, the amplitude A in Eq. (5) will be fixed to a set of discrete values A_n, as well as the oscillation phase. It is a typical demonstration of the discrete energy levels for the macroscopic mechanical resonator in Fig. 1.

In view of the above observation, one could put forward a general question: What happens if the frequencies of the two driving fields are different by any integer multiples of the mechanical frequency

$$|\Delta_2 - \Delta_1| = k\omega_m, \tag{8}$$

where $k = 1, 2, 3, 4, \ldots$?

Figures 3(a)–(d) present four representative illustrations for such frequency combinations. Though the evolutions under different drive amplitudes E evolve to the same average positions of $\langle \mathcal{E}_m(t) \rangle$ in all situations (the illustrations display the stable oscillations on the first energy level), only under the combination $(\Delta_1 = 0, \Delta_2 = \omega_m)$ in Fig. 3(a) can the stabilized oscillations be locked to the same phases. The complete locking of the mechanical oscillation only exists with a combination satisfying $|\Delta_2 - \Delta_1| = \omega_m$, a detuning difference or frequency difference by exact one mechanical frequency, while the partial locking to the first energy level manifests for all illustrated combinations. Other combinations such as those under the conditions $|\Delta_2 - \Delta_1| = 5\omega_m, 6\omega_m$ have been examined to achieve the partial locking only. The existence of the complete and partial locking scenarios is summarized in Table I.

The drive-frequency difference by the integer multiples of ω_m is the prerequisite to all locking scenarios. Even the partial locking to the fixed amplitudes will be gone when there is a small mismatch between two drive frequencies, e.g., the frequency combination becomes $(\Delta_1 = m\omega_m, \Delta_2 = n\omega_m + \delta)$, where δ is a small shift while m and n are two integers. Two examples are given by Figs. 4(a)–4(d), respectively, to show that the tendency of evolving to the same average position $\langle \mathcal{E}_m(t) \rangle$ for the different drive amplitudes E will disappear with the increase of the frequency shift δ. One observation is that, to a larger k in the combinations of $|\Delta_2 - \Delta_1| = k\omega_m$, the energy levels are more robust under the deviation of one drive frequency; the amplitude locking for the combinations satisfying $|\Delta_2 - \Delta_1| = \omega_m$, as exemplified by the combination $(\Delta_1 = 0, \Delta_2 = -\omega_m)$ in Figs. 4(a) and 4(b), is easy to destroy by a slight shift $\delta \sim 0.01\kappa$ (note that $\omega_m = 20\kappa$ in the examples).

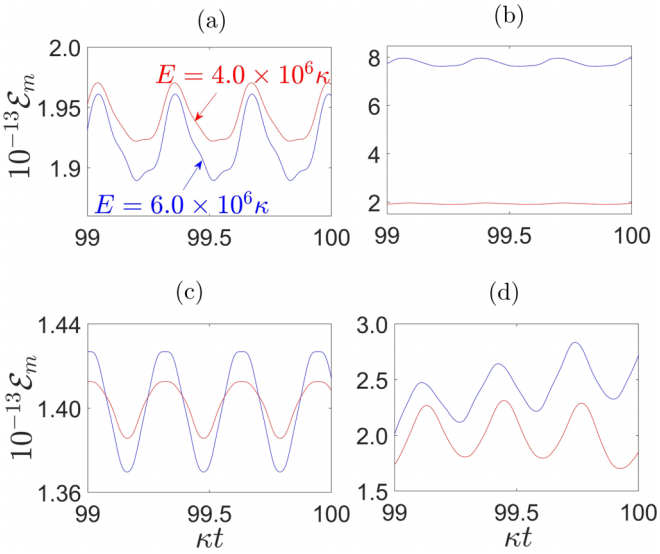

FIG. 4. Loss of the amplitude locking by the mismatch of two drive frequencies: (a) $\Delta_1 = 0$ and $\Delta_2 = -\omega_m + 0.05\kappa$, (b) $\Delta_1 = 0$ and $\Delta_2 = -\omega_m + 0.06\kappa$, (c) $\Delta_1 = -\omega_m$ and $\Delta_2 = 2\omega_m + 0.1\kappa$, and (d) $\Delta_1 = -\omega_m$ and $\Delta_2 = 2\omega_m + 1.0\kappa$. The tendency of destroying the amplitude locking is shown for the combinations (a) and (b) $(\Delta_1 = 0, \Delta_2 = -\omega_m)$ and (c) and (d) $(\Delta_1 = -\omega_m, \Delta_2 = 2\omega_m)$. The sample drive amplitudes in the figures are the same as in (a) and the system parameters are the same as those in Fig. 2.

B. Parallel displaced drive frequencies

The locking phenomena will disappear if one of the driving fields is shifted in its frequency. However, they will be well preserved under the condition that both fields are shifted together by the same amount δ:

$$\Delta_1 \to \Delta_1 + \delta, \quad \Delta_2 \to \Delta_2 + \delta. \tag{9}$$

The examples in Figs. 3(e)–(h) exhibit this feature, which is one of the most fascinating for the nonlinear dynamical scenarios. The dynamical equations (2) are not invariant under such parallel displacement of the drive frequencies, but the same locking phenomenon under a specific drive condition is nonetheless realized after such a displacement, possibly at the cost of a higher drive power. Compared with the amplitude-locking phenomenon in Fig. 3(c), the same type of locking is realized after a displacement over ω_m in Fig. 3(g). Suppose that the highest pump power that is sustainable for a setup corresponds to the amplitude $E_{\max}$ for each driving field; the allowed displacement δ for preserving the complete or partial locking has a certain range for a specific drive condition $|\Delta_2 - \Delta_1| = k\omega_m$. Some examples are given in Fig. 5. The allowed displacement ranges can be extended further with an increased $E_{\max}$ for the setup. The existence of the complete locking after the parallel displacement under the condition $|\Delta_2 - \Delta_1| = \omega_m$ significantly generalizes the same dynamical scenario reported in Ref. [59].

For the purpose of realizing an amplitude locking, one can simply start from a resonant driving field with $\Delta = 0$. Once its drive power is sufficiently high, the amplitude locking in the form of the energy levels in Fig. 2(a) will manifest. Then one continues to shift the drive frequency from the point

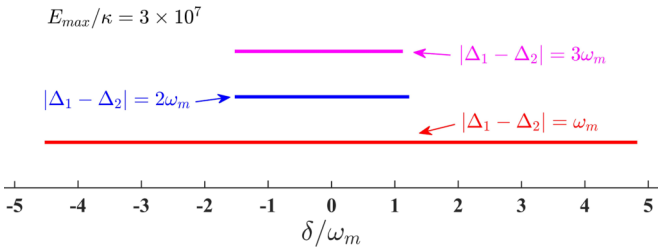

FIG. 5. Examples of the allowed parallel displacement ranges for the specified drive conditions. The locking phenomena will be preserved under the displacement within the ranges. Here the maximum drive amplitude is $E_{\max} = 3\times10^7\kappa$. The system parameters are the same of those in Fig. 2.

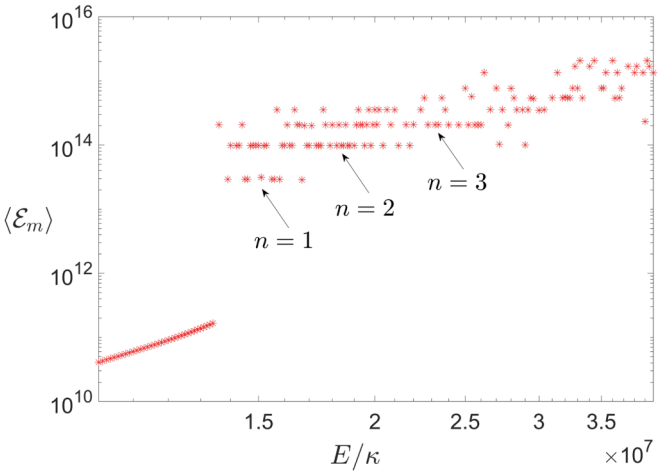

FIG. 6. Energy levels formed due to the driving fields of the combination $(\Delta_1 = -\omega_m, \Delta_2 = \omega_m)$. The threshold for reaching the energy levels is higher than other combinations, and the first three energy levels appear with the same scale of E. The system parameters in Fig. 2 are used here to produce the energy levels displayed with a logarithmic coordinate.

$\Delta = 0$, either to the blue-detuned or to the red-detuned side, and will find that those energy levels will gradually disappear and turn into something like energy bands (the mechanical energy evolved in oscillation is distributed over much wider ranges) in the process of deviating the drive frequency. At this time, the addition of any other driving field with its frequency differing from the previous one by some integer multiples of the mechanical frequency ω_m can restore the energy levels, which are located at the different positions according to the required drive amplitude E. Certainly the pump powers need to be adjusted during the process. This process could be viewed as a self-organization of the OMS, a few-body system with only four degrees of freedom. In the well-known process of optical lasing, the transition from the irregular light of a lamp to the highly ordered light from a laser takes place when the external pumping power is beyond a threshold. The pump power is a control parameter for locking the emission from a multitude of atoms (molecules) to the same pattern. For the present scenarios we consider, two control parameters (the pump power and the drive-frequency difference) work together to bring about the locking phenomena in a few-body system. A higher order of phase locking also manifests when the frequency parameter is adjusted to have $|\Delta_2 - \Delta_1| = \omega_m$.

C. Special energy-level pattern

Now we look at a special combination of the driving fields with $(\Delta_1 = -\omega_m, \Delta_2 = \omega_m)$. Previously, the pumping by one blue-detuned driving field together with another red-detuned driving field was mostly studied for a configuration in which they are applied to two different optical cavities, respectively, and the mechanical resonator in the middle is under the radiation pressure from two different cavities (see, e.g., [81–86]). In that scenario a time-independent steady state will be reached to simplify the description. The difference in the process considered herein is that the two fields pump the same optical cavity simultaneously. According to the linearized dynamics, the former driving field $(\Delta_1 = -\omega_m)$ realizes a resonantly enhanced two-mode squeezing effect to heat up the mechanical motion, but the latter $(\Delta_2 = \omega_m)$ induces the optimum cooling effect on the mechanical oscillator, which has been verified by experiments [18–31]. The joint action of these two conflicting factors can bring about an unusual effect in the nonlinear regime.

With the increase of the drive amplitude $E_1 = E_2 = E$, the mechanical motion initially responds in a linear way, having its stabilized oscillation amplitude grow continuously with E. The conflicting roles of the two driving fields make this linear response period much longer than other drive-frequency combinations. During this period the two competing factors simply balance at the end of a dynamical evolution. However, there will be a sudden transition to the phase of amplitude locking when the driving fields become even stronger, though the threshold for entering the locking phase should be high for this particular drive-frequency combination. Compared to the thresholds $E \approx 1.5\times10^6\kappa$ for a single resonant field and $E \approx 5\times10^5\kappa$ for the combination $(\Delta_1 = 0, \Delta_2 = \omega_m)$, the amplitude locking will occur at $E \approx 1.35\times10^7\kappa$, obtained with the same set of system parameters as in Fig. 2. An interesting feature is that the amplitude locking manifests as a sudden jump into the energy levels (see Fig. 6). This is in sharp contrast to the gradual transition to the first energy level as shown in Fig. 2. Moreover, across the tipping point to the amplitude-locking phase, the first three mechanical levels manifest almost together and the random transition due to a slight variation of E constantly takes place between them. The character of phase transition due to two competing factors is the most obvious in the locking phenomena induced by the combination $(\Delta_1 = -\omega_m, \Delta_2 = \omega_m)$ of the driving fields.

V. LOCKING PHENOMENA IN COUPLED-CAVITY SYSTEMS

The other kind of OMS in Fig. 1(b) has an excitable breathing mode on a microresonator. Such a microresonator can be coupled with others, to make interesting setups such as parity-time symmetric couplers and phonon lasers (see, e.g., [87–98]). Here we take a look at the locking phenomena in this type of coupled system. The difference from the previously discussed scenarios is an extra coupling to another

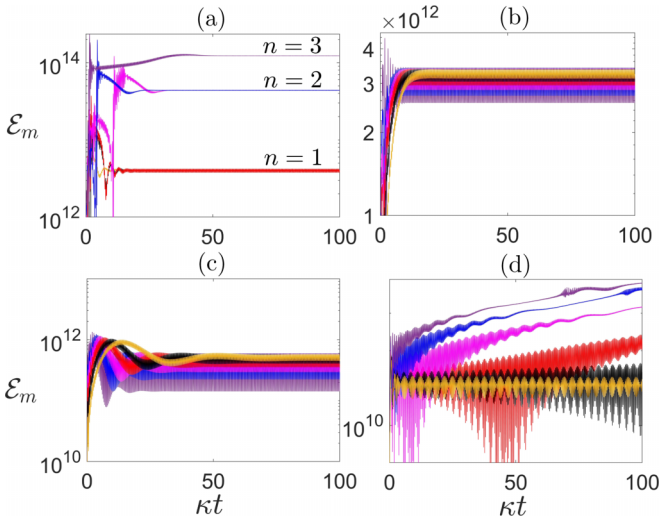

FIG. 7. Dynamical evolutions of the mechanical motions under the driving fields of the combination ($\Delta_1 = 0$, $\Delta_2 = \omega_m$), which act on a number of coupled-cavity systems, for (a) $J = 1.0\kappa$, (b) $J = 5.0\kappa$, (c) $J = 10\kappa$, and (d) $J = 20\kappa$. The drive amplitudes, ranging from $E/\kappa = 5.1\times10^6$ to 9.1×10^6 with an increase of 8×10^5 for each step, are indicated by the yellow, black, red, pink, blue, and indigo curves for the evolving courses. In (a) the yellow, red, and black curves evolve to the first energy level, the pink and blue curves to the second level, and the indigo curve to the third energy level. The energy levels are shown with a logarithmic scale. Increasing the coupling strength J gradually destroys the energy levels. The other parameters are the same as those in Fig. 2.

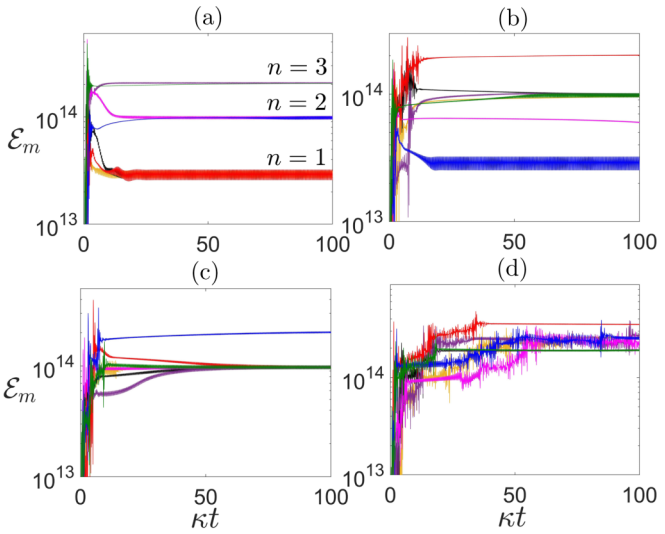

FIG. 8. Dynamical evolutions of the mechanical motions under the driving fields of the combination ($\Delta_1 = -\omega_m$, $\Delta_2 = \omega_m$) for (a) $J = 1.0\kappa$, (b) $J = 5.0\kappa$, (c) $J = 10\kappa$, and (d) $J = 20\kappa$. The drive amplitudes, ranging from $E = 1.39\times10^7\kappa$ to $1.69\times10^7\kappa$ with an even step $5\times10^5\kappa$, are indicated with the yellow, black, indigo, pink, red, blue, and green curves for the evolving courses. In (a) the yellow, black, and red curves evolve to the first energy level, the pink and blue curves to the second level, and the green and indigo curves to the third level. A higher E does not necessarily give a higher energy level here. The other parameters are the same as those in Fig. 2.

microcavity. This mutual coupling between two microcavities, as seen in the interaction potential [Eq. (3)] and the dynamical equations [Eq. (4)], is a linear one. This linear coupling competes with the nonlinear optomechanical interaction in one of the microcavities, leading to a sudden transition of the mechanical oscillation excited by one blue-detuned field [58]. The locked mechanical motion to the energy levels for a single microresonator can be also changed by a gradually increased coupling strength J, and this will be our primary concern.

The first example we examine is the combination ($\Delta_1 = 0$, $\Delta_2 = \omega_m$), one resonant field driving simultaneously with another red-detuned field. We choose a number of evenly distributed drive amplitudes E, which make the system of a single cavity evolve to the first three energy levels, respectively. When the coupling intensity J is increased to 1.0κ for the coupled system, these energy levels will still be preserved as shown in Fig. 7(a). The energy levels created by the driving fields of the combination ($\Delta_1 = 0$, $\Delta_2 = \omega_m$) can be easily destroyed by the mismatch of the drive frequencies [59], but here we see that they are more robust under the coupling with another cavity. Over a considerable range of coupling intensity J, the optomechanical effect in the system becomes rather stable; the values of the mechanical energy stimulated by various drive amplitudes go together to form an energy band as in Figs. 7(b) and 7(c). As the coupling J becomes still larger, there is a tendency for the system to reduce to a quasilinear one. In Fig. 7(d) the finally evolved phonon number shows a tendency of linear response to the external drive intensity; a higher value of the stabilized energy will be obtained due to a higher mechanical energy magnitudes E. Note that the mechanical energy magnitudes finally stabilized in Fig. 7(d), especially the red, pink, blue, and indigo ones, are not on energy levels but are simply the samples in a continuous distribution, because the evolved curve due to an in-between drive amplitude will be located somewhere between these curves. By energy levels we mean that the averages of the evolved mechanical energy are located only at fixed values and the oscillation amplitudes of the stabilized mechanical energy are small, irrespective of the drive amplitude E.

The special energy-level structure due to the combination ($\Delta_1 = -\omega_m$, $\Delta_2 = \omega_m$) is our second example. The influence on such energy levels by the coupling strength is illustrated in Fig. 8. A special feature for this type of energy level is that the evolved mechanical energy loses the monotonic relation with the drive amplitude E as seen from the regime of amplitude locking in Fig. 6, where the energy levels seemingly overlap. For instance, in Fig. 8(a) the red curve due to a drive amplitude higher than the pink one can go to the first energy level, while the pink one evolves to the second level. The further increased coupling J will deform the energy levels and make the evolutions more irregular [see Figs. 8(b)–(d)]. Because the optomechanical interaction is generally stronger in this scenario, i.e., the drive amplitude should be much higher to see the energy levels and other nonlinear effects, the system still demonstrates a nonlinear behavior in Fig. 8(d), without being reduced to a quasilinear one by a comparable intercavity coupling as in Fig. 7(d).

VI. CONCLUSION

The numerical simulations based on Eqs. (2) and (4) were implemented with the computation platforms MATLAB (ODE45 and other solvers) and *Mathematica*. For the locking phenomena on the first energy level ($n = 1$), any chosen computation accuracy does not generally influence the simulation results. In the regime of higher energy levels, however, different choices of accuracy in the numerical calculation may lead a dynamical evolution to different energy levels, but the simulated result always ends in one of the determined energy levels without going elsewhere. This is similar to the action of noise perturbations [99,100] that exist in the realistic systems and induce the random transitions between the higher energy levels (the regime with the irregular distribution of the energy levels with the drive amplitude E). The noise perturbations can be simulated with the respective random drive terms in the dynamical equations and they will not influence the dynamical behavior after the system stabilizes [59]. The target of our present study is to illustrate the locking patterns for the stabilized mechanical oscillation, which are the same on each energy level and irrelevant to the final state a system would evolve to. Therefore, we here neglect the noise perturbations and simply demonstrate the locking patterns with the first level $n = 1$. For the possible experimental realization of the locking phenomena, the threshold drive intensity is an important concern. The driving fields with the combinations ($\Delta_1 = 0, \Delta_2 = \omega_m$) and ($\Delta_1 = 0, \Delta_2 = -\omega_m$) are the best candidates, since their required threshold intensities for entering the first energy level are the lowest.

In the present work we demonstrated that the mechanical motion in an OMS can be locked under various drive conditions. The driving fields detuned at the red-detuned resonant point $\Delta = \omega_m$ and the blue-detuned resonant point $\Delta = -\omega_m$ were highly interesting in the previous study of OMSs, as the former is the optimum one for implementing optomechanical cooling and the latter is used to obtain the best two-mode squeezing effect for achieving optomechanical entanglement. Through numerical simulations we found that all detuning points at $k\omega_m$, where k includes both negative and positive integers, as well as $k = 0$, were special to an OMS. The stabilized oscillation of an OMS driven by a resonant field can display amplitude locking. Whenever this OMS is driven by a field detuned at some other integer multiples $l\omega_m$ of the mechanical frequency, its stable oscillation amplitude can also be locked if one more driving field detuned at a different multiple of the mechanical frequency $n\omega_m$ is added and the enhanced drive power is sustainable for the setup. Interestingly, the frequencies of the two fields can be shifted together to see the same amplitude locking, as long as the drive power is correspondingly adjusted. Given a special combination in which the frequencies of the two driving fields differ exactly by the mechanical frequency, both the amplitude and phase of a stabilized oscillation can be fixed to realize a complete locking. More features and possible applications of the locking phenomena await further exploration.

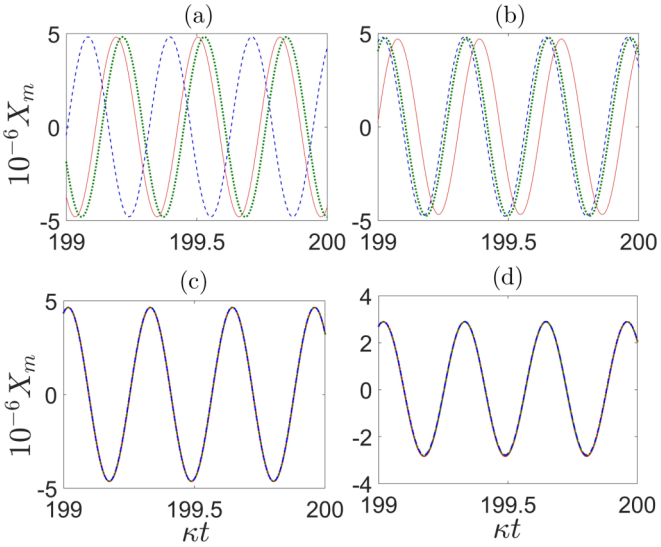

FIG. 9. From amplitude locking to phase locking. Here we consider a drive frequency combination ($\Delta_1 = 0, \Delta_2 = \omega_m$) for two driving fields with their amplitudes E_1 and E_2: (a) $E_2 = 0$, (b) $E_2 = 0.02E_1$, (c) $E_2 = 0.09E_1$, and (d) $E_2 = E_1$. (a) Only under one driving field of resonance ($E_2 = 0$), the amplitudes of the stabilized mechanical oscillations X_m become the same for three different driving fields with $E_1 = 4\times10^6\kappa$ (red solid curve), $E_1 = 5\times10^6\kappa$ (green dotted curve), and $E_1 = 6\times10^6\kappa$ (indigo dashed curve). All these mechanical oscillations are locked to the same amplitude since the driving fields are stronger than the threshold, though the mechanical oscillation phase varies with E. (b)–(d) The gradual increase of the cooling field will lock the oscillation phase. The locked mechanical oscillation amplitude is also minimized when the cooling field is enhanced to $E_2 = E_1$. All other parameters are the same as those in Fig. 2.

ACKNOWLEDGMENTS

This work was supported by National Natural Science Foundation of China (Grant No. 11574093) and Natural Science Foundation of Fujian Province of China (Grant No. 2020J01061).

APPENDIX A: ALTERNATIVE PRESENTATION OF THE LOCKING PHENOMENA

In the main text we displayed the locking phenomena in terms of the evolved mechanical energy or phonon number $\mathcal{E}_m$, because different drive amplitudes E give rise to the varied pure displacements d of the mechanical resonator and so the corresponding amplitudes $A_n d$ of the stabilized $\mathcal{E}_m(t)$ can be well distinguished even though the oscillation amplitudes A_n are locked. For a direct demonstration of the amplitude- and phase-locking scenarios, we illustrate here the locking processes in terms of the stabilized mechanical displacement $X_m(t)$.

We first start from the action of single resonant driving field in Fig. 9. Because the involved drive amplitudes surpass the threshold to form the first energy level, all stabilized $X_m(t)$ have the same amplitude as it is locked by a nonlinear mechanism. From such a state of amplitude locking, we add another driving field red detuned at $\Delta = \omega_m$ and gradually enhance its intensity. Then the phase of all stabilized oscillations $X_m(t)$ will tend to be locked too, even given a red-detuned field not so strong [$E_2 = 0.09E_1$ in Fig. 9(c)]. The further enhanced

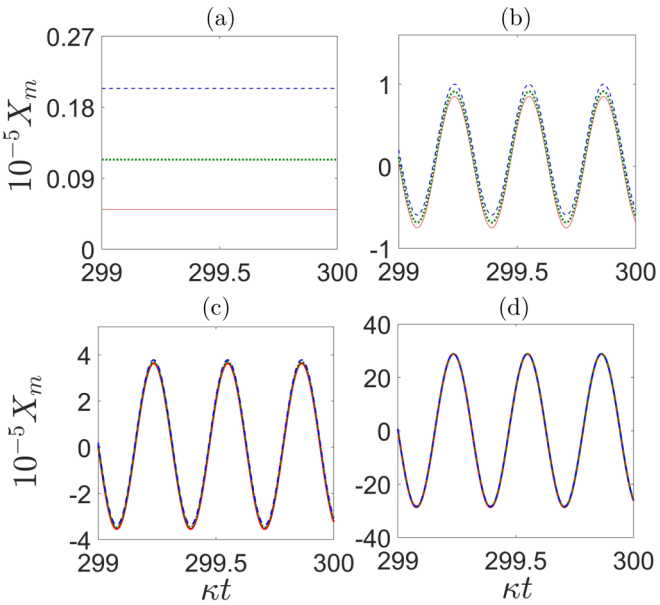

FIG. 10. From cooling to complete locking. Here we consider a drive frequency combination ($\Delta_1 = \omega_m, \Delta_2 = 0$) for two driving fields with their amplitudes E_1 and E_2: (a) $E_2 = 0$, (b) $E_2 = 0.02E_1$, (c) $E_2 = 0.09E_1$, and (d) $E_2 = E_1$. (a) Only under one cooling field ($E_2 = 0$), the mechanical motion X_m finally stops at a time-independent steady state with a pure displacement d from the equilibrium position without radiation pressure [one has $A = 0$ but $d \neq 0$ in Eq. (5)]. Here three different drive amplitudes, $E_1 = 2\times10^6\kappa$ (red solid curve), $E_1 = 3\times10^6\kappa$ (green dotted curve), and $E_1 = 4\times10^6\kappa$ (indigo dashed curve), are used to show such displacements. (b)–(d) The gradual increase of the resonant field will drive the mechanical resonator into oscillation and gradually lock both oscillations to the same amplitude and phase. The mechanical oscillation amplitude is also increased together with the enhancement of the resonant field. All other parameters are the same as those in Fig. 2.

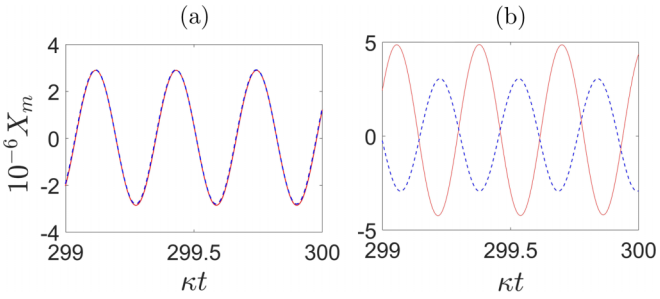

FIG. 11. Disappearance of the locking phenomena due to violation of a frequency-matched condition for (a) $\Delta_1 = 0$ and $\Delta_2 = \omega_m + 0.05\kappa$ and (b) $\Delta_1 = 0$ and $\Delta_2 = \omega_m + 0.4\kappa$. Here $E_1 = E_2 = 4\times10^6\kappa$ (red solid curve) and $E_1 = E_2 = 6\times10^6\kappa$ (indigo dashed curve). (a) The mechanical oscillations are still locked approximately if the frequency of the cooling field is shifted by a very small amount. (b) Both amplitude locking and phase locking will be lost after the cooling field has more frequency shift. The system parameters are the same as those in Fig. 2.

red-detuned field (the cooling field) will decrease the amplitudes of $X_m(t)$ to the minimum when it becomes as strong as the resonant one ($E_2 = E_1$). The complete locking of the oscillation amplitude and phase makes the evolved $X_m(t)$ look the same. For this reason we used the evolved mechanical energy in the main text to distinguish between the locked mechanical motion for different drive amplitudes E.

Another interesting scenario results from the cooling by a single red-detuned field, which renders the mechanical oscillator at a standstill in the end. The equilibrium positions d realized by the exemplary drive amplitudes in Fig. 10(a) are simply the samples among a continuum distribution; the other values of E between them will fill the gaps between any two of these exemplary drive amplitudes. By adding another resonant field, one will see that the stabilized mechanical motion becomes oscillatory, as in Fig. 10(b). The tendency in the process of enhancing the resonant field is that all stabilized oscillations will have the same amplitude and phase, realizing a complete locking of the mechanical oscillation. Meanwhile the oscillation amplitude (or the mechanical energy) is increased by the gradually strengthened resonant field. For all different drive amplitudes E within a certain range, the stabilized mechanical oscillations will have the same amplitude A_1 corresponding to the energy $\langle \mathcal{E}_m(t) \rangle \approx A_1^2/2$ on the first energy level, as long as the two drive frequencies satisfy the condition $|\Delta_2 - \Delta_1| = \omega_m$.

In contrast, the amplitude and phase locking will gradually disappear if the drive frequencies deviate from the condition $|\Delta_1 - \Delta_2| = \omega_m$. One example is in Fig. 11, where the drive frequency combination ($\Delta_1 = 0, \Delta_2 = \omega_m$) is still considered. When the red-detuned cooling field deviates a little from the point $\Delta_1 = \omega_m$ ($\delta = 0.05\kappa$) as in Fig. 11(a), the mechanical oscillations due to different drive amplitudes E are still locked approximately, unless a further refined scale or a detailed spectrum analysis of the cavity field is applied to view the stabilized states. However, a continual increase of the frequency deviation (for example, $\delta = 0.4\kappa$) will destroy both phase locking and amplitude locking as in Fig. 11(b). This is an alternative way to Fig. 4 for illustrating the loss of locking phenomena by a drive frequency shift.

[1] M. Aspelmeyer, T. J. Kippenberg, and F. Marquardt, Cavity optomechanics, Rev. Mod. Phys. **86**, 1391 (2014).

[2] I. Wilson-Rae, N. Nooshi, W. Zwerger, and T. J. Kippenberg, Theory of Ground State Cooling of a Mechanical Oscillator Using Dynamical Backaction, Phys. Rev. Lett. **99**, 093901 (2007).

[3] F. Marquardt, J. P. Chen, A. A. Clerk, and S. M. Girvin, Quantum Theory of Cavity-Assisted Sideband Cooling of Mechanical Motion, Phys. Rev. Lett. **99**, 093902 (2007).

[4] F. Marquardt, A. A. Clerk, and S. M. Girvin, Quantum theory of optomechanical cooling, J. Mod. Opt. **55**, 3329 (2008).

[5] C. Genes, D. Vitali, P. Tombesi, S. Gigan, and M. Aspelmeyer, Ground-state cooling of a micromechanical oscillator: Comparing cold damping and cavity-assisted cooling schemes, Phys. Rev. A **77**, 033804 (2008).

[6] A. Dantan, C. Genes, D. Vitali, and M. Pinard, Self-cooling of a movable mirror to the ground state using radiation pressure, Phys. Rev. A **77**, 011804(R) (2008).

[7] J. M. Dobrindt, I. Wilson-Rae, and T. J. Kippenberg, Parametric Normal-Mode Splitting in Cavity Optomechanics, Phys. Rev. Lett. **101**, 263602 (2008).

[8] P. Rabl, C. Genes, K. Hammerer, and M. Aspelmeyer, Phase-noise induced limitations on cooling and coherent evolution in optomechanical systems, Phys. Rev. A **80**, 063819 (2009).

[9] Y. Li, L. A. Wu, Y. D. Wang, and L. P. Yang, Nondeterministic ultrafast ground-state cooling of a mechanical resonator, Phys. Rev. B **84**, 094502 (2011).

[10] X. T. Wang, S. Vinjanampathy, F. W. Strauch, and K. Jacobs, Ultraefficient Cooling of Resonators: Beating Sideband Cooling with Quantum Control, Phys. Rev. Lett. **107**, 177204 (2011).

[11] Y. C. Liu, Y.-F. Xiao, X. Luan, and C. W. Wong, Dynamic Dissipative Cooling of a Mechanical Resonator in Strong Coupling Optomechanics, Phys. Rev. Lett. **110**, 153606 (2013).

[12] Y. C. Liu, Y. W. Hu, C. W. Wong, and Y. F. Xiao, Review of cavity optomechanical cooling, Chin. Phys. B **22**, 114213 (2013).

[13] B. He, L. Yang, Q. Lin, and M. Xiao, Radiation Pressure Cooling as a Quantum Dynamical Process, Phys. Rev. Lett. **118**, 233604 (2017).

[14] Q. Lin and B. He, Highly efficient cooling of mechanical resonator with square pulse drives, Opt. Express **26**, 33830 (2018).

[15] C. Wang, Q. Lin, and B. He, Breaking the optomechanical cooling limit by two drive fields on a membrane-in-the-middle system, Phys. Rev. A **99**, 023829 (2019).

[16] D.-G. Lai, J.-F. Huang, X.-L. Yin, B.-P. Hou, W. Li, D. Vitali, F. Nori, and J.-Q. Liao, Nonreciprocal ground-state cooling of multiple mechanical resonators, Phys. Rev. A **102**, 011502(R) (2020).

[17] Z.-X. Chen, B. He, and Q. Lin, Efficient ground state cooling of a membrane by the combination of continuous-wave field and pulses, J. Phys. B **54**, 095502 (2021).

[18] J. D. Teufel, J. W. Harlow, C. A. Regal, and K. W. Lehnert, Dynamical Backaction of Microwave Fields on a Nanomechanical Oscillator, Phys. Rev. Lett. **101**, 197203 (2008).

[19] S. Gröblacher, J. B. Hertzberg, M. R. Vanner, S. Gigan, K. C. Schwab, and M. Aspelmeyer, Demonstration of an ultracold micro-optomechanical oscillator in a cryogenic cavity, Nat. Phys. **5**, 485 (2009).

[20] A. Schliesser, O. Arcizet, R. Riviére, G. Anetsberger, and T. J. Kippenberg, Resolved-sideband cooling and position measurement of a micromechanical oscillator close to the Heisenberg uncertainty limit, Nat. Phys. **5**, 509 (2009).

[21] Y.-S. Park and H. Wang, Resolved-sideband and cryogenic cooling of an optomechanical resonator, Nat. Phys. **5**, 489 (2009).

[22] A. D. O'Connell, M. Hofheinz, M. Ansmann, R. C. Bialczak, M. Lenander, E. Lucero, M. Neeley, D. Sank, H. Wang, M. Weides, J. Wenner, J. M. Martinis, and A. N. Cleland, Quantum ground state and single-phonon control of a mechanical resonator, Nature (London) **464**, 697 (2010).

[23] T. Rocheleau, T. Ndukum, C. Macklin, J. B. Hertzberg, A. A. Clerk, and K. C. Schwab, Preparation and detection of a mechanical resonator near the ground state of motion, Nature (London) **463**, 72 (2010).

[24] R. Riviére, S. Delèglise, S. Weis, E. Gavartin, O. Arcizet, A. Schliesser, and T. J. Kippenberg, Optomechanical sideband cooling of a micromechanical oscillator close to the quantum ground state, Phys. Rev. A **83**, 063835 (2011).

[25] J. D. Teufel, T. Donner, D. Li, J. H. Harlow, M. S. Allman, K. Cicak, A. J. Sirois, J. D. Whittaker, K. W. Lehnert, and R. W. Simmonds, Sideband cooling of micromechanical motion to the quantum ground state, Nature (London) **475**, 359 (2011).

[26] J. Chan, T. P. M. Alegre, A. H. Safavi-Naeini, J. T. Hill, A. Krause, S. Gröblacher, M. Aspelmeyer, and O. Painter, Laser cooling of a nanomechanical oscillator into its quantum ground state, Nature (London) **478**, 89 (2011).

[27] M. H. Schleier-Smith, I. D. Leroux, H. Zhang, M. A. Van Camp, and V. Vuletić, Optomechanical Cavity Cooling of an Atomic Ensemble, Phys. Rev. Lett. **107**, 143005 (2011).

[28] E. Verhagen, S. Delèglise, S. Weis, A. Schliesser, and T. J. Kippenberg, Quantum-coherent coupling of a mechanical oscillator to an optical cavity mode, Nature (London) **482**, 63 (2012).

[29] A. H. Safavi-Naeini, J. Chan, J. T. Hill, T. P. M. Alegre, A. Krause, and O. Painter, Observation of Quantum Motion of a Nanomechanical Resonator, Phys. Rev. Lett. **108**, 033602 (2012).

[30] R. W. Peterson, T. P. Purdy, N. S. Kampel, R. W. Andrews, P.-L. Yu, K. W. Lehnert, and C. A. Regal, Laser Cooling of a Micromechanical Membrane to the Quantum Backaction Limit, Phys. Rev. Lett. **116**, 063601 (2016).

[31] J. B. Clark, F. Lecocq, R. W. Simmonds, J. Aumentado, and J. D. Teufel, Sideband cooling beyond the quantum backaction limit with squeezed light, Nature (London) **541**, 191 (2017).

[32] D. Vitali, S. Gigan, A. Ferreira, H. R. Böhm, P. Tombesi, A. Guerreiro, V. Vedral, A. Zeilinger, and M. Aspelmeyer, Optomechanical Entanglement between a Movable Mirror and a Cavity Field, Phys. Rev. Lett. **98**, 030405 (2007).

[33] M. Paternostro, D. Vitali, S. Gigan, M. S. Kim, C. Brukner, J. Eisert, and M. Aspelmeyer, Creating and Probing Multipartite Macroscopic Entanglement with Light, Phys. Rev. Lett. **99**, 250401 (2007).

[34] D. Vitali, P. Tombesi, M. J. Woolley, A. C. Doherty, and G. J. Milburn, Entangling a nanomechanical resonator and a superconducting microwave cavity, Phys. Rev. A **76**, 042336 (2007).

[35] C. Genes, A. Mari, P. Tombesi, and D. Vitali, Robust entanglement of a micromechanical resonator with output optical fields, Phys. Rev. A **78**, 032316 (2008).

[36] M. J. Hartmann and M. B. Plenio, Steady State Entanglement in the Mechanical Vibrations of Two Dielectric Membranes, Phys. Rev. Lett. **101**, 200503 (2008).

[37] C.-L. Zou, X.-B. Zou, F.-W. Sun, Z.-F. Han, and G.-C. Guo, Room-temperature steady-state optomechanical entanglement on a chip, Phys. Rev. A **84**, 032317 (2011).

[38] M. Abdi, S. Barzanjeh, P. Tombesi, and D. Vitali, Effect of phase noise on the generation of stationary entanglement in cavity optomechanics, Phys. Rev. A **84**, 032325 (2011).

[39] Q. Lin, B. He, R. Ghobadi, and C. Simon, Fully quantum approach to optomechanical entanglement, Phys. Rev. A **90**, 022309 (2014).

[40] Q. Lin and B. He, Optomechanical entanglement under pulse drive, Opt. Express **23**, 24497 (2015).

[41] Z.-X. Chen, Q. Lin, B. He, and Z.-Y. Lin, Entanglement dynamics in double-cavity optomechanical systems, Opt. Express **25**, 17237 (2017).

[42] T. A. Palomaki, J. D. Teufel, R. W. Simmonds, and K. W. Lehnert, Entangling Mechanical Motion with Microwave Fields, Science **342**, 710 (2013).

[43] S. G. Hofer, W. Wieczorek, M. Aspelmeyer, and K. Hammerer, Quantum entanglement and teleportation in pulsed cavity optomechanics, Phys. Rev. A **84**, 052327 (2011).

[44] M. R. Vanner, I. Pikovski, G. D. Cole, M. S. Kim, C. Brukner, K. Hammerer, G. J. Milburn, and M. Aspelmeyer, Pulsed quantum optomechanics, Proc. Natl. Acad. Sci. USA **108**, 16182 (2011).

[45] M. R. Vanner, J. Hofer, G. D. Cole, and M. Aspelmeyer, Cooling-by-measurement and mechanical state tomography via pulsed optomechanics, Nat. Commun. **4**, 2295 (2013).

[46] A. A. Rakhubovsky and R. Filip, Robust entanglement with a thermal mechanical oscillator, Phys. Rev. A **91**, 062317 (2015).

[47] Q. Lin, B. He, and M. Xiao, Entangling Two Macroscopic Mechanical Resonators at High Temperature, Phys. Rev. Appl. **13**, 034030 (2020).

[48] K. Y. Dixon, L. Cohen, N. Bhusal, C. Wipf, J. P. Dowling, and T. Corbitt, Optomechanical entanglement at room temperature: A simulation study with realistic conditions, Phys. Rev. A **102**, 063518 (2020).

[49] W. H. Zurek, Decoherence, einselection, and the quantum origins of the classical, Rev. Mod. Phys. **75**, 715 (2003).

[50] A. J. Leggett and A. Garg, Quantum Mechanics versus Macroscopic Realism: Is the Flux There When Nobody Looks? Phys. Rev. Lett. **54**, 857 (1985).

[51] A. J. Leggett, Testing the limits of quantum mechanics: motivation, state of play, prospects, J. Phys.: Condens. Matter **14**, R415 (2002).

[52] B. He, Quantum optomechanics beyond linearization, Phys. Rev. A **85**, 063820 (2012).

[53] T. Carmon, H. Rokhsari, L. Yang, T. J. Kippenberg, and K. J. Vahala, Temporal Behavior of Radiation-Pressure-Induced Vibrations of an Optical Microcavity Phonon Mode, Phys. Rev. Lett. **94**, 223902 (2005).

[54] H. Rokhsari, T. Kippenberg, T. Carmon, and K. Vahala, Radiation-pressure-driven micro-mechanical oscillator, Opt. Express **13**, 5293 (2005).

[55] F. Marquardt, J. G. E. Harris, and S. M. Girvin, Dynamical Multistability Induced by Radiation Pressure in High-Finesse Micromechanical Optical Cavities, Phys. Rev. Lett. **96**, 103901 (2006).

[56] M. Ludwig, B. Kubala, and F. Marquardt, The optomechanical instability in the quantum regime, New J. Phys. **10**, 095013 (2008).

[57] A. G. Krause, J. T. Hill, M. Ludwig, A. H. Safavi-Naeini, J. Chan, F. Marquardt, and O. Painter, Nonlinear Radiation Pressure Dynamics in an Optomechanical Crystal, Phys. Rev. Lett. **115**, 233601 (2015).

[58] Q. Lin, B. He, and M. Xiao, Catastrophic transition between dynamical patterns in a phonon laser, Phys. Rev. Res. **3**, L032018 (2021).

[59] B. He, Q. Lin, M. Orszag, and M. Xiao, Mechanical oscillations frozen on discrete levels by two optical driving fields, Phys. Rev. A **102**, 011503(R) (2020).

[60] S. H. Strogatz and I. Stewart, Coupled oscillators and biological synchronization, Sci. Am. **269**, 102 (1993).

[61] A. Pikovsky, M. Rosenblum, and J. Kurths, *Synchronization: A Universal Concept in Nonlinear Sciences* (Cambridge University Press, Cambridge, 2001).

[62] R. V. Jensen, Synchronization of driven nonlinear oscillators, Am. J. Phys. **70**, 607 (2002).

[63] A. Balanov, N. Janson, D. Postnov, and O. Sosnovtseva, *Synchronization: From Simple to Complex* (Springer, Berlin, 2009).

[64] C. Huygens, *Horologium Oscillatorium* (Muguet, Paris, 1673).

[65] M. G. Rosenblum, A. S. Pikovsky, and J. Kurths, Phase Synchronization of Chaotic Oscillators, Phys. Rev. Lett. **76**, 1804 (1996).

[66] G. V. Osipov, B. Hu, C. Zhou, M. V. Ivanchenko, and J. Kurths, Three Types of Transitions to Phase Synchronization in Coupled Chaotic Oscillators, Phys. Rev. Lett. **91**, 024101 (2003).

[67] F. Dörfler and F. Bullo, Synchronization in complex networks of phase oscillators: A survey, Automatica **50**, 1539 (2014).

[68] J. Gómez-Gardeñes, Y. Moreno, and A. Arenas, Paths to Synchronization on Complex Networks, Phys. Rev. Lett. **98**, 034101 (2007).

[69] J. Gómez-Gardeñes, S. Gómez, A. Arenas, and Y. Moreno, Explosive Synchronization Transitions in Scale-Free Networks, Phys. Rev. Lett. **106**, 128701 (2011).

[70] J. R. Terry, K. S. Thornburg, Jr., D. J. DeShazer, G. D. Vanwiggeren, S. Zhu, P. Ashwin, and R. Roy, Synchronization of chaos in an array of three lasers, Phys. Rev. E **59**, 4036 (1999).

[71] M. C. Cross, A. Zumdieck, R. Lifshitz, and J. L. Rogers, Synchronization by Nonlinear Frequency Pulling, Phys. Rev. Lett. **93**, 224101 (2004).

[72] H. F. Chen and J. M. Liu, Complete phase and amplitude synchronization of broadband chaotic optical fields generated by semiconductor lasers subject to optical injection, Phys. Rev. E **71**, 046216 (2005).

[73] S. Yanchuk, K. Schneider, and O. Lykova, Amplitude synchronization in a system of two coupled semiconductor lasers, Ukr. Math. J. **60**, 495 (2008).

[74] A. B. Tort, R. Komorowski, H. Eichenbaum, and N. Kopell, Measuring phase-amplitude coupling between neuronal oscillations of different frequencies, J. Neurophysiol. **104**, 1195 (2010).

[75] R. T. Canolty and R. T. Knight, The functional role of cross-frequency coupling, Trends Cognitive Sci. **14**, 506 (2010).

[76] J. Fell and N. Axmacher, The role of phase synchronization in memory processes, Nat. Rev. Neurosci. **12**, 105 (2011).

[77] M. H. Matheny, M. Grau, L. G. Villanueva, R. B. Karabalin, M. C. Cross, and M. L. Roukes, Phase Synchronization of Two Anharmonic Nanomechanical Oscillators, Phys. Rev. Lett. **112**, 014101 (2014).

[78] F. Böhm, A. Zakharova, E. Schöll, and K. Lüdge, Amplitude-phase coupling drives chimera states in globally coupled laser networks, Phys. Rev. E **91**, 040901(R) (2015).

[79] J. M. González-Miranda, Amplitude envelope synchronization in coupled chaotic oscillators, Phys. Rev. E **65**, 036232 (2002).

[80] Q. Qiu, B. Z. Zhou, P. Wang, L. G. He, Y. H. Xiao, Z. Y. Yang, and M. Zhan, Origin of amplitude synchronization in coupled nonidentical oscillators, Phys. Rev. E **101**, 022210 (2020).

[81] P. Meystre, E. M. Wright, J. D. McCullen, and E. Vignes, Theory of radiation-pressure-driven interferometers, J. Opt. Soc. Am. B **2**, 1830 (1985).

[82] M. Bhattacharya and P. Meystre, Trapping and Cooling a Mirror to Its Quantum Mechanical Ground state, Phys. Rev. Lett. **99**, 073601 (2007)

[83] A. M. Jayich, J. C. Sankey, B. M. Zwickl, C. Yang, J. D. Thompson, S. M. Girvin, A. A. Clerk, F. Marquardt, and J. G. E. Harris, Dispersive optomechanics: A membrane inside a cavity, New J. Phys. **10**, 095008 (2008).

[84] Y. Li, L. A. Wu, and Z. D. Wang, Fast ground-state cooling of mechanical resonators with time-dependent optical cavities, Phys. Rev. A **83**, 043804 (2011).

[85] M. Karuza, C. Molinelli, M. Galassi, C. Biancofiore, R. Natali, P. Tombesi, G. Di Giuseppe, and D. Vitali, Optomechanical sideband cooling of a thin membrane within a cavity, New J. Phys. **14**, 095015 (2012)

[86] Y. J. Guo, K. Li, W. J. Nie, and Y. Li, Electromagnetically-induced-transparency-like ground-state cooling in a double cavity optomechanical system, Phys. Rev. A **90**, 053841 (2014).

[87] J. Wen, X. Jiang, L. Jiang, and M. Xiao, Parity-time symmetry in optical microcavity systems, J. Phys. B **51**, 222001 (2018).

[88] R. El-Ganainy, K. G. Makris, M. Khajavikhan, Z. H. Musslimani, S. Rotter, and D. N. Christodoulides, Non-Hermitian physics and $\mathcal{PT}$ symmetry, Nat. Phys. **14**, 11 (2018).

[89] B. He, L. Yang, Z. Zhang, and M. Xiao, Cyclic permutation-time symmetric structure with coupled gain-loss microcavities, Phys. Rev. A **91**, 033830 (2015).

[90] I. S. Grudinin, H. Lee, O. Painter, and K. J. Vahala, Phonon Laser Action in a Tunable Two-Level System, Phys. Rev. Lett. **104**, 083901 (2010).

[91] H. Jing, S. K. Özdemir, X. Y. Lü, J. Zhang, L. Yang, and F. Nori, $\mathcal{PT}$-Symmetric Phonon Laser, Phys. Rev. Lett. **113**, 053604 (2014).

[92] B. He, L. Yang, and M. Xiao, Dynamical phonon laser in coupled active-passive microresonators, Phys. Rev. A **94**, 031802(R) (2016).

[93] H. Lü, S. K. Özdemir, L.-M. Kuang, F. Nori, and H. Jing, Exceptional Points in Random-Defect Phonon Lasers, Phys. Rev. Appl. **8**, 044020 (2017).

[94] Y. L. Zhang, C. L. Zou, C. S. Yang, H. Jing, C. H. Dong, G. C. Guo, and X. B. Zou, Phase-controlled phonon laser, New J. Phys. **20**, 093005 (2018).

[95] B. Wang, H. Xiong, X. Jia, and Y. Wu, Phonon laser in the coupled vector cavity optomechanics, Sci. Rep. **8**, 282 (2018).

[96] Y. F. Xie, Z. Cao, B. He, and Q. Lin, $\mathcal{PT}$-symmetric phonon laser under gain saturation effect, Opt. Express **28**, 22580 (2020).

[97] G. Z. Wang, M. M. Zhao, Y. C. Qin, Z. Q. Yin, X. S. Jiang, and M. Xiao, Demonstration of an ultra-low-threshold phonon laser with coupled microtoroid resonators in vacuum, Photon. Res. **5**, 73 (2017).

[98] J. Zhang, B. Peng, Ş. K. Özdemir, K. Pichler, D. O. Krimer, G. P. Zhao, F. Nori, Y. X. Liu, S. Rotter, and L. Yang, A phonon laser operating at an exceptional point, Nat. Photon. **12**, 479 (2018).

[99] C. W. Gardiner and P. Zoller, *Quantum Noise* (Springer, Berlin, 2000).

[100] W. Horsthemke and R. Lefever, *Noise-Induced Transitions* (Springer, Berlin, 2006).